

# An 8 GeV Linac as the Booster Replacement in the Fermilab Power Upgrade

*S. Belomestnykh, M. Checchin, D. Johnson, D. Neuffer, S. Posen, E. Pozdeyev,  
V. Pronskikh, N. Solyak, V. Yakovlev*

*Fermilab, PO Box 500, Batavia IL 60510 USA*

**Abstract.** Increasing the Main Injector (MI) beam power above  $\sim 1.2$  MW requires replacement of the 8 GeV Booster by a higher intensity alternative. In the Project X era, rapid-cycling synchrotron (RCS) and Linac solutions were considered for this purpose. In this paper, we consider the Linac version that produces 8 GeV H<sup>+</sup> beam for injection into the Recycler Ring (RR) or Main Injector (MI). The Linac takes  $\sim 1$  GeV beam from the PIP-II Linac and accelerates it to  $\sim 2$  GeV in a 650 MHz SRF Linac, followed by a  $\sim 2$ -8 GeV pulsed Linac using 1300 MHz cryomodules. The Linac components incorporate recent improvements in SRF technology. The Linac configuration and beam dynamics requirements are presented. Injection options are discussed. Foil-based injection is the present standard but R&D toward implementing laser-assisted injection could enable a significant improvement. Research needed to implement the Booster replacement is described.

Keywords: Linac, beams, PIP-II.

## INTRODUCTION

The PIP-II project will provide a 800 MeV proton beam with CW capability, with beam power up to the MW level available for user experiments [1]. However, the amount of beam that can be transmitted to the Main Injector (MI) is limited by the 0.8—8.0 GeV Booster capacity. The next Fermilab upgrade should include a replacement for the Booster. The project-X design proposal included some options for that replacement, based on a continuation of the 800 MeV Linac to 2—3 GeV followed by either a Rapid Cycling Synchrotron (RCS) or continuing the Linac to 8 GeV [2]. An 8 GeV Linac may be made relatively affordable by extending the use of 650 MHz PIP-II cryomodules and adding relatively inexpensive ILC-style cryomodules that use 1300 MHz SRF cavities, that have already been designed and mass-produced for the European XFEL and LCLS-II machines

In this note we focus on the 8 GeV Linac option. We begin with some discussion of the beam requirements and potential layouts for the Linac. Constraints on accelerating gradients and magnetic fields are discussed. The Project X 8 GeV design is used as an initial template.

## LINAC SCENARIO REQUIREMENTS

The Fermilab Proton Improvement Plan II (PIP-II) provides a new 800 MeV superconducting RF (SRF) Linac that replaces the previous 400 MeV Linac, enabling higher intensity injection into the Fermilab Booster and providing 800 MeV proton beam to other experiments. The primary purpose of PIP-II is to provide enhanced beam power delivery from the Main Injector (MI) to DUNE (Deep Underground Neutrino Experiment). This is enabled by increasing the beam energy and intensity delivered by the Linac to the Fermilab Booster and increasing the Booster cycle rate, thereby increasing injected beam into the MI. Table 1 shows high-level parameters of the Fermilab beam to DUNE before and after PIP-II, as presented in the Fermilab PIP-II Design Report. PIP-II increases the Booster cycle rate to 20 Hz and the beam intensity to  $6.6 \times 10^{12}$  protons/pulse, enabling MI beam power of  $\sim 1 - 1.2$  MW at beam energies of 60 to 120 GeV.

With the completion of PIP-II, the 60-years-old Booster becomes the limiting bottleneck in providing MI beam to DUNE, and further improvements will require replacement of the Booster with a higher-capacity injector. This Booster

Replacement (BR) should provide substantially higher intensity to DUNE. The initial design specification for the BR upgrade is that it should enable at least  $\sim 2.4$  MW from the MI. High-level performance goals for a Booster Replacement Linac (BRL) are presented in Table I. The BRL parameters presented there should be considered as initial goals for the BRL project. The BRL project should be capable of significant extension beyond these initial goals, and these potential improvements may influence the BRL design development.

**Table 1:** High level performance goals for PIP, PIP-II, and Booster Replacement Linac (BRL)

<b>Performance Parameter</b>	<b>PIP</b>	<b>PIP-II</b>	<b>BRL</b>	<b>Unit</b>
Linac Beam Energy	400	800	8000	MeV
Linac Beam Current (chopped)	25	2	2	mA
Linac Pulse Length	0.03	0.54	2.2	ms
Linac Pulse Repetition Rate	15	20	20	Hz
Linac Upgrade Potential	N/A	CW	CW	
8 GeV Protons per Pulse (extracted)	4.2	6.5	27.5	$10^{12}$
8 GeV Pulse Repetition Rate	15	20	20	Hz
Beam Power @ 8 GeV	80	166	700	kW
8 GeV Beam Power to MI	50	83-142*	176-300	kW
Beam Power to 8 GeV Program (pulsed mode)	30	83-24*	500-375	kW
Main Injector Protons per Pulse (extracted)	4.9	7.5	15.6	$10^{13}$
Main Injector Cycle Time @ 120 GeV	1.33	1.2	1.2	s
Main Injector Cycle Time @ 60 GeV	N/A	0.7	0.7	s
Beam Power @ 60 GeV	N/A	1	2.15	MW
Beam Power @ 120 GeV	0.7	1.2	2.5	MW

\*Total PIP-II with Booster 8 GeV power is 166 kW.

Booster replacement was considered by the Project X research program and both Linac and Recycling Synchrotron versions were developed [2]. The parameters for BRL shown in Table 1 are based in part on the Project X parameters, updated to follow recently developed requirements.

Fig. 1 shows a potential layout for the BRL, based upon the Project-X design. The 800 MeV Linac is extended to  $\sim 1$  GeV. The beam exiting that Linac is bent away from the Main Injector by  $\sim 45^\circ$  into a 1 $\rightarrow$ 3 GeV Linac, consisting of 650 MHz cryomodules ( $\sim 280$  m long). This is followed by a  $105^\circ$  bend, that bends the beam back toward the Main Injector. A  $\sim 390$ m long Linac, consisting of 1300 MHz cryomodules accelerates the beam from 3 to 8 GeV, and a following short transport injects the  $H^-$  beam into the Recycler Ring directly above the Main Injector, where charge exchange injection accumulates protons, for transfer into the Main Injector. Parameters of the Linac components are shown in Table 2. The curves away and back toward the Main Injection are required to fit the relatively long Linac sections into the short space between the PIP-II Linac and the Main Injector.

This Project X scenario will be considered as an initial guide toward constructing the 8 GeV Linac version presented in this report.

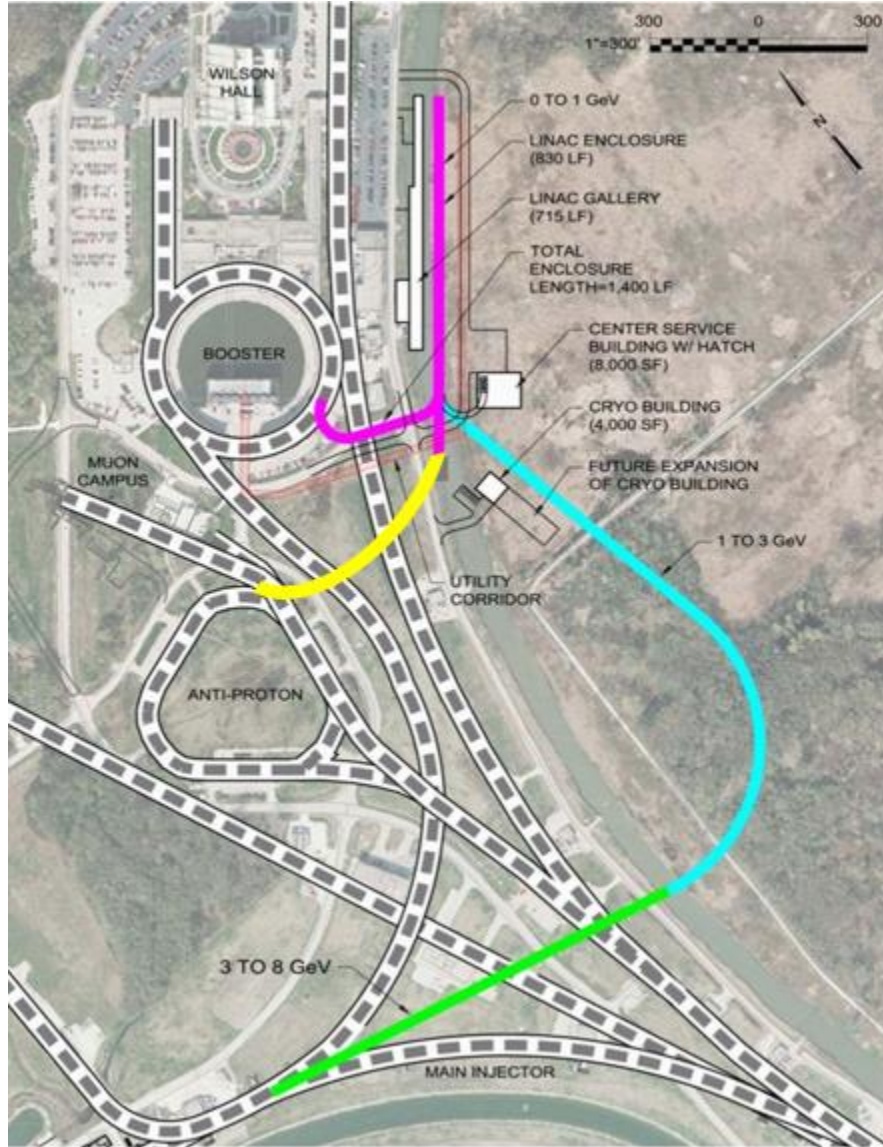


**FIGURE 1.** Layout of the 8 GeV Linac as envisioned in Project X (from ref. 3).

**Table 2:** Parameters of the Project X 8 GeV Linac

Section	Length	Bending field or RF frequency	Total bending angle or Linac mode	Cav/mag /CM	Cryomodule length
1GeV transport	40 m	0.277T	-45°		
1→3 GeV Linac	240m	650 MHz	CW	120/20/ 20	9.92m
3 GeV bend	200m	0.13T	105°		
3→8 GeV Linac	390m	1300 MHz	Pulsed, 10 Hz	224 /28/28	12.5 m
8GeV injection		0.055T			

### Advantages and Disadvantages of a Linac Upgrade

We are considering both Linac and rapid-cycling synchrotron (RCS) versions of the BR. The RCS version is presented in some detail in [4].

Potential advantages of the Linac option include:

- Improvements in SRF technology have greatly reduced the cost of accelerating cavities and modules. 650 MHz cryomodules will be developed for PIP-II and the incremental construction costs of the additional modules of an 8 GeV Linac scenario should be relatively affordable. 1300 MHz modules are being mass produced for electron accelerators. The same modules can be used for high-energy proton acceleration, and these should also be affordable.
- Linac acceleration through to the MI eliminates the need for intermediate injections and accumulator rings, which could simplify construction and operation.
- It should be substantially more efficient than an RCS. An RCS system expends considerable energy in cycling magnets from low to high field and back, in addition to the accelerating RF power requirements. SRF cavities are very efficient in converting RF power into beam energy. This efficiency advantage would be magnified in a higher-power upgrade to CW operation. The Linac system could be upgradeable to a much larger total delivered beam power.
- Many experiments benefit from a CW beam, which is most readily obtained from a CW Linac.
- While a foil-stripping injection may be more difficult at 8 GeV, laser-assisted injection may be easier because lower-frequency lasers can be used.

Potential disadvantages of the Linac option are:

- Requires H<sup>-</sup> injection at 8 GeV into the Main Injector or Recycler Ring. The MI/RR is not designed to include charge exchange injection; modifications are needed.
- H<sup>-</sup> beam at 8 GeV is vulnerable to magnetic stripping, gas stripping and intra-beam stripping.
- The PIP-II to MI geometry is constrained and relatively inflexible. The most natural injection point would be MI-10, which is slated for LBNE extraction. The alternative is RR-10 injection with beam accumulation in the RR, with transfer to the MI. The injection difficulties are discussed in more detail below.
- Many experiments need pulsed beam. This can be obtained by H<sup>-</sup> injection and accumulation into a fixed energy storage ring, at the cost of an added ~8 GeV storage ring. This storage ring could also be used to accumulate beam for injection into the MI, providing an alternative to RR-10 injection.
- It could be more expensive than an RCS alternative; that comparison should be evaluated.
- H<sup>-</sup> injection into a new RCS ring could be more optimized, since a new ring could have straight sections more completely optimized for foil injection. Also, losses would occur with lower energy injected beam rather than 8 GeV Linac injected beam.

## PIP-II LINAC DESIGN AND PARAMETERS

The Booster Replacement Linac would be an extension of the PIP-II Linac [1]. The Proton Improvement Plan-II (PIP-II) encompasses a set of upgrades and improvements to the Fermilab accelerator complex aimed at supporting a world-leading High Energy Physics program over the next several decades. The primary goals for PIP-II are:

- Deliver beam with a power of 1.2 MW to the LBNF/DUNE target, upgradable to multi-MW.
- Deliver a platform capable of high-duty-factor/high-beam-power operations while providing flexible bunch patterns to multiple experiments simultaneously.
- Deliver a platform to support future upgrades of the accelerator complex.
- Ensure sustained high reliability of the Fermilab accelerator complex.
- The above capabilities should be provided in a cost-effective manner.

PIP-II includes a superconducting Linac to fuel the next generation of intensity frontier experiments. The linac will accelerate H<sup>-</sup> ions to 800 MeV for injection into the Booster. The project also includes upgrades to the existing Booster, Main Injector, and Recycler rings that will enable them to operate at an increased repetition rate (Booster at 20 Hz and Main Injector at 0.83 Hz) and deliver a 1.2 MW proton beam to the Long Baseline Neutrino Facility (LBNF) target. Fig. 2 show the PIP-II Linac with the Beam transfer Line to the Fermilab Booster on the campus. Fig. 3 shows the layout of the major Linac components.



FIGURE 2. PIP-II Linac location on Fermilab campus.

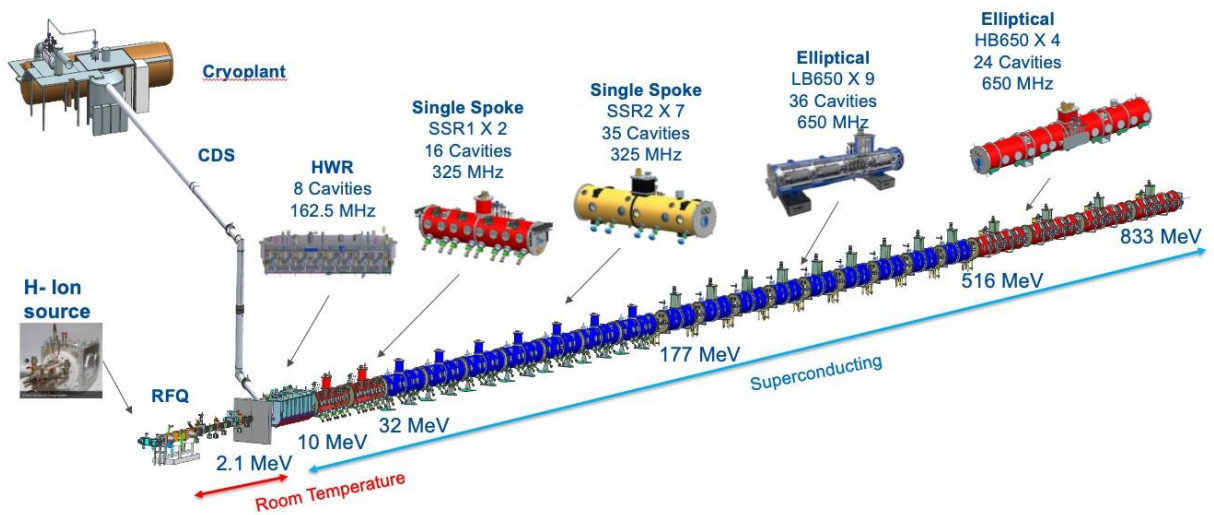


FIGURE 3. PIP-II Linac with the cryo-plant and the cryogenic distribution system (CDS). The Linac consists of the room-temperature front end, one HWR cryomodule, two types of Single-Spoke resonator cryomodules (SSR1 and SSR2), and two types of elliptical cavity cryomodules (LB650 and HB650).

The PIP-II Linac components include:

- **Ion sources and LEBT.** The baseline design of the PIP-II linac includes two identical multi-cusp, filament-driven, H- sources with their own Low Energy Beam Transport (LEBT) branches. A 3-way switching magnet allows fast switching between the sources. The ion sources are designed to operate in the DC regime, producing up to approximately 15 mA of H- beam current.
- **RFQ.** The PIP-II RFQ is a 4-vane brazed structure operating at 162.5 MHz. The RFQ is designed to accelerate the beam to 2.1 MeV in the CW regime. The RFQ sets the minimum temporal separation between bunches in the Linac.

- **MEBT Chopper.** The medium energy beam transport (MEBT) includes a chopper that is designed to selectively remove bunches without affecting neighboring bunches. The chopper can create arbitrarily programmed bunch patterns. The chopper consists of two kickers, a beam absorber, and pulse forming electronics. The beam intensity is reduced by approximately 60% in the MEBT by the fast MEBT chopper and collimators to ensure lossless injection of the 162.5 MHz PIP-II bunch pattern into the 45 MHz RF of the Booster.
- **SRF Linac.** The SRF linac is designed to accelerate H<sup>-</sup> beams and consists of five different types of cavities as show in Fig. 3. The number of cavities and their design are optimized to match the velocity profile of the accelerated H<sup>-</sup> beam. The scope of the PIP-II project includes four HB650 cryomodules, sufficient to accelerate the beam to 833 MeV. The linac tunnel has space for two additional HB650 CMs that can accelerate the beam to 1050 MeV. The design of the RF cavities is optimized for CW operations with a beam intensity of several milliamperes.
- **Beam Transfer Line (BTL).** The PIP-II project includes a beam transfer line (BTL) to deliver the beam from the linac to the Fermilab Booster.

The initial PIP-II design establishes some key features:

- The MEBT chopper can provide arbitrary, programmable bunch patterns, including gaps and reduced frequency. This functionality is critical for PIP-II operations. Because the frequency of the Linac RF is not a harmonic of the Booster RF or the MI RF, a significant portion of the Linac bunches will be lost. The chopper selectively removes bunches that would be injected too close to the separatrix or miss the bucket. Based on simulations of the injection process into the Booster, the chopper will have to remove up to 60% of the bunches. In addition, the chopper will be used to produce flexible bunch patterns required for other users and secondary beam operation.
- The highest bunch frequency is 162.5 MHz, determined by the RFQ. The bunch frequency can be reduced using the MEBT chopper.
- The number of H<sup>-</sup> per bunch can reach  $4 \times 10^8$  without suffering significant degradation of the beam quality. The nominal bunch intensity in the LBNF mode is  $1.9 \times 10^8$  H<sup>-</sup> per bunch.
- The average beam current (over 1  $\mu$ s) is limited to 2 mA ( $1.25 \times 10^{16}$  H<sup>-</sup>/sec) by the RF power available from the RF amplifiers. Any combination of bunch frequency and charge is possible if the average current in the pulse does not exceed 2 mA, the bunch frequency does not exceed 162.5 MHz, and the maximum number of particles per bunch does not exceed  $4 \times 10^8$ .

### PIP-II Science program with beam provided to multiple users

The PIP-II Mission Need Statement (MNS) requires PIP-II to deliver 1.2 MW of the beam power from the MI onto the LBNF target, and to provide beam to other laboratory experiments. The MNS also requires PIP-II to allow a subsequent doubling of beam power delivered from the MI while providing beam to other users for a broader spectrum of particle physics research opportunities. The design of the PIP-II Linac includes provisions that facilitate future upgrades and addition of users. The Booster Replacement program should also provide further opportunities for other users, with the possibility to provide proton beam to new experiments using 1—8 GeV protons.

In addition to the MI program, the PIP-II Linac (with no energy upgrade) can deliver a CW beam with a power of up to 1.6 MW. The MI LBNF/DUNE experiment in the PIP-II era (1.2 MW on the LBNF target) requires only approximately 1.1% of the total potential beam intensity. Even with the doubled beam power on target, the LBNF beam will require only 2.2% of the Linac CW intensity. The rest of the beam can be delivered to multiple users, enabling concurrent operations.

There are two main types of devices that can be used to distribute beam to multiple users:

- **RF Separators** are RF cavities that operate at a subharmonic of the bunch repetition frequency and separate the beam in two or more beamlets. Instead of accelerating the beam, RF separators are designed to provide a

transverse kick using either electric or magnetic RF field. Fig. 4 shows the principle of operation of an RF separator. The kick provided by the separator depends on the bunch arrival phase.

- **Fast Switching magnets** can deflect the beam to required experiments and switch between beam destinations in 10-20 microseconds. Such a magnet can be programmed to switch the beam periodically between multiple users in a quasi-concurrent manner, delivering periodic bursts of beam with the full pulse intensity. The fast MEBT chopper will turn off the beam in the Linac during magnet switching to avoid beam losses.

RF separators and fast switching magnets can be combined in any required combination making PIP-II capable of providing flexible bunch patterns and high duty factor/higher beam power operations to multiple experiments simultaneously.

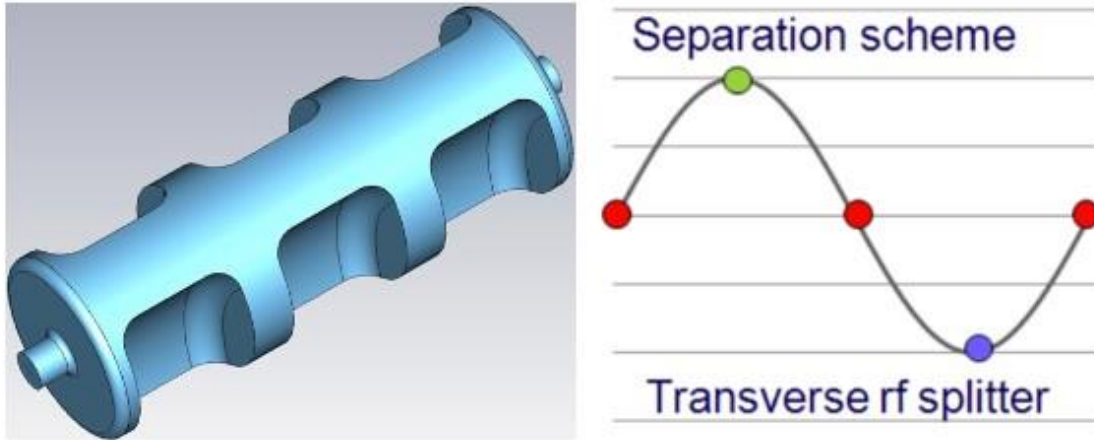


**FIGURE 4.** RF Separator Concept. An RF cavity, operating at a subharmonic of the bunch repetition frequency, is designed to provide a transverse kick. The amplitude and the direction of the deflection angle depend on the phase of bunch arrival in the cavity.

### Intensity Upgrade

To achieve 1.2 MW of beam power on the LBNF target, PIP-II needs to accelerate 550  $\mu\text{s}$ -long pulses with an average peak current of 2 mA. This peak beam intensity is an order of magnitude lower than that in some other pulsed, high-power accelerators such as SNS or ESS. This choice provides several advantages. First, it reduces intensity-dependent effects and alleviates their impact on the beam quality, simplifying beam chopping and allowing for precision painting during injection in the Booster. Second, it allows using widely available, easy-to-operate, CW-capable solid-state amplifiers. On the other hand, the low beam intensity requires longer injection time into the Booster and will require longer injection times for the 8 GeV Linac into the MI. Long injection times can be problematic due to injection foil overheating and cycle timing constraints. Increasing the beam current in the Linac can mitigate these issues.

In considering options for boosting the linac intensity, we divide the intensity increase into two ranges loosely based on the impact on accelerator systems and beam parameters: a moderate increase by roughly a factor of 2 and a substantial increase by a factor of 5 to 10:

**Moderate increase of Linac beam current.** Results of numerical studies and engineering estimates show that increasing the beam current to 4-5 mA, that is, by a factor of 2 to 2.5 relative to the PIP-II baseline design, is feasible without significant design changes and requires only increasing the output power of RF amplifiers roughly proportionally to the beam current. The increased RF power output can affect requirements for the facility electrical power, utilities, and space. Therefore, more compact and efficient amplifier designs shall be evaluated as an alternative to solid state amplifiers.

**Substantial increase of Linac beam current.** An increase of the Linac beam current by a factor of 5 to 10 (from 2 mA to 10 mA to 20 mA) will require more substantial changes to the PIP-II facility. A new ion source and RFQ would be required. Space charge and intra-beam scattering will become important limitations in operation. RF amplifiers, power supplies and couplers will need to be upgraded; the linac will require significant modifications to be able to operate with 10-20 mA beams. In the present study we will limit consideration to moderate increase scenarios.

## BRL SCENARIO DESCRIPTION

The PIP-II Linac provides the basis for the Booster Replacement Linac scenarios. In this section we describe a baseline approach for the BRL, starting from the current established PIP-II location. Fig. 5 shows the layout, which is similar to one considered in the Project X era, and Table 3 summarizes the component parameters. The initial PIP-II Linac can be extended to 1 GeV extraction, by inserting additional cryomodules in existing space at the end of the PIP-II Linac. A switching magnet at that point bends the beam into a curved channel (away from the Booster toward Fermilab Project South). This curved channel bends the beam by  $\sim 45^\circ$ , leading into a 650 MHz Linac which takes the beam to 2.4 GeV. This is followed by a  $105^\circ$  curved transport that directs the beam into a 1300 MHz Linac that accelerates the beam to 8.0 GeV. This is followed by a final transport that matches the  $H^-$  beam into the recycler at RR-10.

In our initial configuration, the beam pulse structure is similar to that for the PIP-II Booster injection. The beam current is pulsed at 20 Hz, with each pulse  $\sim 2.1$  ms long and the beam current is chopped from 5 mA to 2 mA to match the  $\sim 53$  MHz pattern of beam injected into the MI/RR. 6 pulses of the  $H^-$  beam are used to fill the RR in preparation for transfer to the Main Injector and acceleration. The MI cycle is designed to cycle in 1.2 s to 120 GeV for extraction toward the LBNF target, resulting in  $\sim 2.5$  MW power of beam on target for the DUNE neutrino beam. (An alternative cycle of 0.7 s at 60 GeV (2.2 MW) will also be possible.)

In this initial pulsed configuration, only  $\frac{1}{4}$  of the 20 Hz pulses are directed toward the RR/MI, and the remaining pulses could be directed toward other experiments using 8 GeV proton beam, or beam could be extracted at intermediate energies, such as 2.4 GeV. The PIP-II Linac is capable of CW operation, and the BRL 650 and 1300 MHz Linacs could also be upgraded to CW, if the physics program demands it.

### Transport from PIP-II

The Transport from PIP-II is initiated by a fast switching magnet that deflects the beam into a transport section that bends the beam by  $45^\circ$  and directs it into the first Linac section. The transport would be an achromat of 4  $90^\circ$  cells, similar to that used for transport into the Booster.

### 650 MHz Linac

In the geometry of Fig. 5, the Linac section between the arcs is  $\sim 290$  m long, and it is designed to accelerate the beam to an intermediate energy before it is directed into the final Linac section. The value of that intermediate energy will depend upon demand for physics at that energy as well as cost and performance optimization. Another consideration is to keep the energy low enough to avoid magnetic stripping in the  $105^\circ$  bend toward the MI. Values of 2—3 GeV for this transition have been considered, with the higher value limited by the magnetic stripping and the lower value by cost optimization and the threshold for Kaon production. In our initial example we have chosen 2.4 GeV as a reference case.

The linac could be composed of 650 MHz or 1300 MHz RF, with the transition occurring at an optimum energy. Previous studies conducted to compare the efficiency of HB650 and TESLA 1.3 GHz cryomodules for the Linac extension concluded that 650 MHz HB650 cavities and cryomodules were more efficient below 2 GeV, and possibly as high as 3 GeV. By the time the PIP-II energy upgrade will be ready to be implemented, the design and performance of the HB650 cryomodule and its cavities will be validated and significant experience with their manufacturing, testing, and operation will be obtained, so a more precise optimum could be determined. Recent advances in the 1300 MHz SRF technology for CW operation in LCLS-II will be taken into account as well. To simplify the initial configuration of the BRL, the 650 MHz PIP-II cryomodules are chosen for this entire segment, see Fig. 5.

Acceleration to  $\sim 2.4$  GeV requires 1.4 GeV of acceleration from 1 GeV (or 1.6 GeV from 0.8 GeV). PIP-II cryomodules should be capable of at least 120 MV. With additional R&D focused on the 650 MHz cavities, we can expect improvements in both accelerating gradients and intrinsic quality factors. For this exercise we assume modest improvements of accelerating gradients to 22.6 MV/m (which should give us an energy gain of approximately

140 MeV per cryomodule) with quality factors of  $6.0 \times 10^{10}$ , so 10 (or 12) cryomodules will certainly be adequate. Each cryomodule is 9.9 m long, and in PIP-II the cryomodules are in an 11.8 m lattice with a quadrupole doublet between each module. For this Linac a single quad per module would be used, so the lattice could be a bit more compact. 10—12 modules with the 11.82 m period requires 120 – 145 m, which fits into the 290 m slot, with at least 140 m of transport available, which can be used for optics matching and collimation, as well as elements to enable extraction into an external beam facility.

The initial configuration is for a pulsed linac, focused on the needs of the neutrino program from the Main Injector, and uses the same 20 Hz repetition rate used for PIP-II injection into the Booster. It is also compatible with a CW Linac with energies up to  $\sim 2.5$  GeV. The end of the Linac could include pulsed kickers and/or RF separators to transport beam into a new intensity frontier facility in this vicinity, where pulsed or CW beam could feed a new family of experiments.

### Transport to final linac

Following the 650 MHz Linac the beamline must be bent and directed toward the RR-10 injection. The total bend is  $105^\circ$ , and a  $\sim 165$  m long transport is needed to ensure that magnetic stripping of 2.4 GeV  $H^-$  does not occur. This would be obtained by a 8-cell FODO achromat ( $720^\circ$  phase advance). The bend will include momentum collimation to reduce losses in the 1300 MHz Linac and injection.

### 1300 MHz Pulsed Linac

After the  $105^\circ$  bend, there is a 510 m long transport, which must include the  $2.4 \rightarrow 8$  GeV 1300 MHz RF plus optical matching and the final transport into the RR. The Linac would contain LCLS-II style cryomodules, operating in pulsed mode. Each of these is  $\sim 12.5$  m long and includes 8 cavities and a focusing quad. Each cryomodule could provide at least 200 MeV of CW acceleration, with a mean accelerating gradient of  $\sim 25$  MV/m.  $\sim 28$  of these cryomodules would be needed, which implies a 350 m long Linac. With some space reserved for matching optics, we can allot  $\sim 410$  m for the Linac, leaving  $\sim 100$  m for the final transport matching into the RR. This is somewhat more space constrained than the 650 MHz Linac.

The LCLS-II cryomodules can operate in CW mode if required by experiments. However, if only pulsed mode of operation is considered, we can raise the accelerating gradient from 25 MV/m to 35.5 MV/m or even higher, and then obtain more than  $\sim 280$  MeV per cryomodule. In that case, only  $\sim 20$  cryomodules will be required, which is reflected in Table 3, as our baseline scenario. This will significantly shorten the Linac to 250 meters. We reserve an additional 50 m in Table 3 for optical elements.

### Match into Recycler /MI

We have reserved  $\sim 150$  m out of  $\sim 200$  m from the end of the Linac for the transport into RR-10 injection. This section must include matching optics, including final bending into the RR, with the injection chicane magnets. Bending fields must be less than  $\sim 0.05$  T to avoid stripping.

This 200 m section could also include RF separators or pulsed kickers into a beam line for a separate 8 GeV experimental facility. This new facility may prefer CW beam, which would require upgrading the 1300 MHz linac. Otherwise, a pulsed beam program using 20 Hz cycles not needed for the MI program could be developed.

**Table 3:** Components of the 8 GeV Linac scenario. Geometry is similar to the Project X case.

Section	Length	RF frequency or bending field	Total bending angle or Linac operation	Cav/mag /CM	Cryomodule length
1GeV transport	32 m	0.25T	$-45^\circ$		
$1 \rightarrow 2.4$ GeV Linac	290 m	650 MHz	CW or 20 Hz	60/10/10	9.92m
2.4 GeV bend	165 m	0.13T	$105^\circ$		
$2.4 \rightarrow 8$ GeV Linac	310 m	1300 MHz	Pulsed, 20 Hz	160 /20/20	12.5 m
8GeV injection	200 m	0.05T			

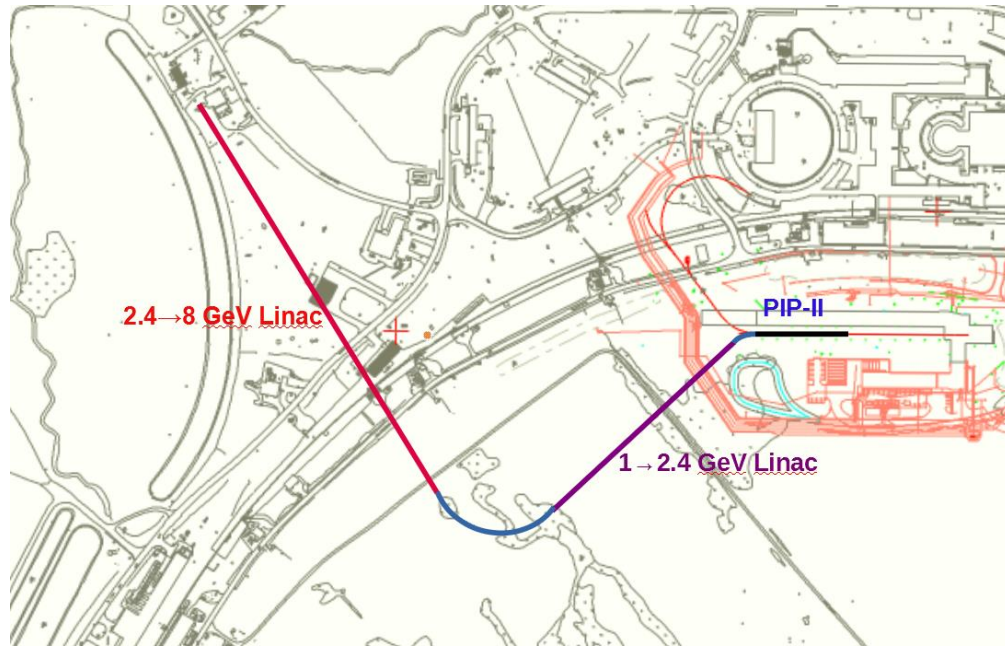


**FIGURE 5.** Layout of the 8 GeV Linac of Table 3 superimposed on a recent PIP-II layout map; note similarities to Fig. 1.

**Table 4:** BRL Linac SRF system parameters

Parameter	650 MHz	1300 MHz
Geometric $\beta$	0.92	1.0
Cells per cavity	5	9
Cavity length $l$	1.061 m	1.038 m
$R/Q$	610 $\Omega$	1036 $\Omega$
$G = Q_0 \times R_s$	255 $\Omega$	270 $\Omega$
Accelerating gradient $E_{acc}$	22.6 MV/m	35.5 MV/m
$E_{pk}$	46.8 MV/m	71 MV/m
$B_{pk}$	87.9 mT	151 mT
$Q_0$	$6.0 \times 10^{10}$	$2.0 \times 10^{10}$
Beam current	2-5 mA	2-5 mA
$Q_L$	$0.7-2.0 \times 10^7$	$0.7-1.7 \times 10^7$
Losses at 2 K	15.7 W	65.5 W (pulsed)
Cavity RF power	120 kW	184 kW
Cavities per cryomodule	6	8
Cryomodule length	9.9 m	12.5 m

## SRF CAVITIES AND CRYOMODULES

The demonstrated and projected performance of SRF cavities and systems has significantly changed since Project X. Two major discoveries at Fermilab have greatly improved SRF cavity performance [5, 6]. First, nitrogen

doping of SRF cavities has been shown to reduce the BCS surface resistance below previously perceived limits. Second, effective magnetic flux expulsion by fast, high thermal gradient, cooldown has achieved record low residual resistances. These innovations combined with continuing optimization of cavity treatments have greatly increased useable gradients, with increased Q values. Most recently, a 75/120°C modified low temperature bake improved Q by ~50%, and increased RF gradient to ~50 MV/m for 1300 MHz cavities [7]. These improvements should be incorporated into the BRL design, and are considered in the SRF parameters presented in Table 4. Continued research in the Booster Replacement program could obtain substantially greater improvements.

### Cryomodule parameters

The building blocks for linac construction are the HB650 MHz cryomodules, developed for PIP-II, and the 1300 MHz cryomodules, developed for the ILC (for pulsed operation) and the LCLS-II project at SLAC (for CW operation) [8]. These designs are relatively advanced, and can be implemented for BRL with minimal modifications. Cross sections of a 650 MHz and a 1300 MHz cryomodule are shown in Figs. 6 and 7, respectively.

The 650 MHz cryomodule contains six 1.064 m long cavities within a total length of ~9.9 m. An accelerating gradient of  $E_{acc} = 18.8$  MV/m, yields an acceleration of 120 MeV per cryomodule. Upgrading this to ~22.6 MV/m yields ~140 MV of acceleration, which could be available for the Booster Replacement Linac with modest investments in R&D.

The 1300 MHz cryomodule contains eight 1.038 m cavities, which are included in a ~12.5 m length. This would provide ~200 MeV at 24 MV/m (slightly improved LCLS-II-HE technology). An upgrade to 35.5 MV/m (R&D on ILC technology, currently in progress) would increase that to ~295 MeV, which is what is used in our initial scenario. Future study would determine an optimum gradient. The gradient must not be above thresholds for H<sup>-</sup> stripping.

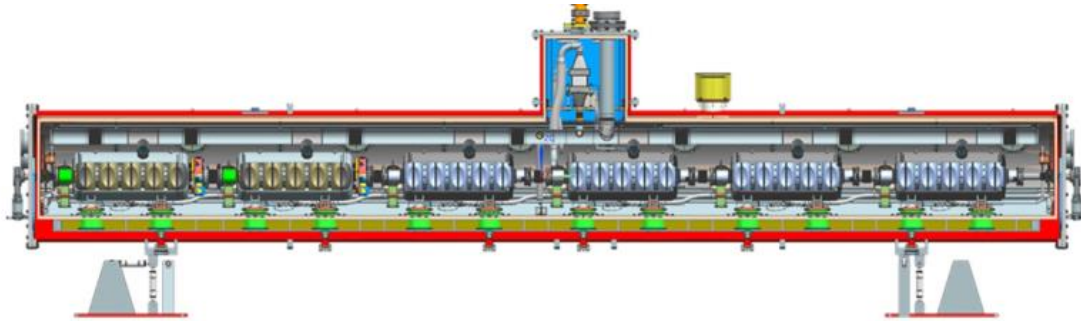


**FIGURE 6:** Cross section of a 9.9 m long 650 MHz cryomodule, containing 6 5-cell RF cavities.

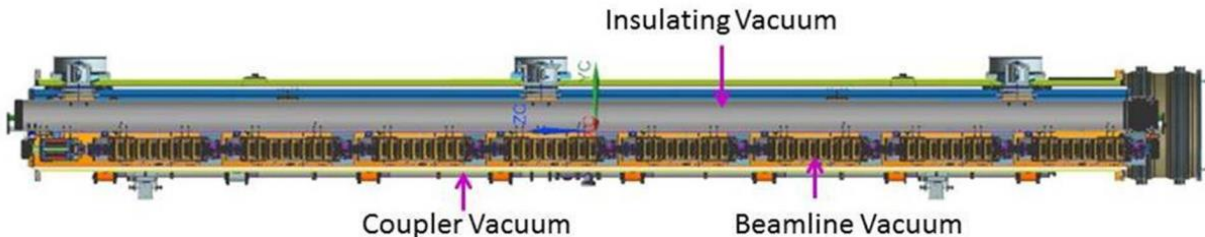


**FIGURE 7:** Cross section of a 12.5 m long 1300 MHz cryomodule, containing 8 9-cell cavities, a focusing magnet, from the LCLS-II design [10].

### Cavity properties and constraints

The PIP-II HB650 cavity ( $\beta_G = 0.92$ ) is a 5-cell elliptical SRF cavity operating at 650 MHz. For the BRL 1 → 2.4 GeV Linac we assume that the cavity will provide an energy gain of 24 MeV to H<sup>-</sup> beam. The cavities will operate with an intrinsic quality factor of  $6.0 \times 10^{10}$  at 2 K. The cell shape optimizes the ratio of the peak surface magnetic and electric fields,  $H_{peak}$  and  $E_{peak}$ , to the accelerating gradient,  $E_{acc}$ . The cavity iris aperture was chosen at 118 mm as a compromise between the peak field ratios, shunt impedance, cell-to-cell coupling, and cavity handling

during processing. The beam tube inner diameter is 117.77 mm and has penetrations for the fundamental power coupler (FPC), which is centered 96 mm from the end iris to provide  $Q_{ext} = 0.7 - 2.0 \times 10^7$ , and for the pickup probe at the other end of the structure. Fig. 8 show a mechanical drawing of the HB650 cavity. See Table 4 for a listing of the HB650 cavity electromagnetic parameters. If necessary, a  $\beta = 1$  version of HB650 cavity can easily be derived from the existing design.

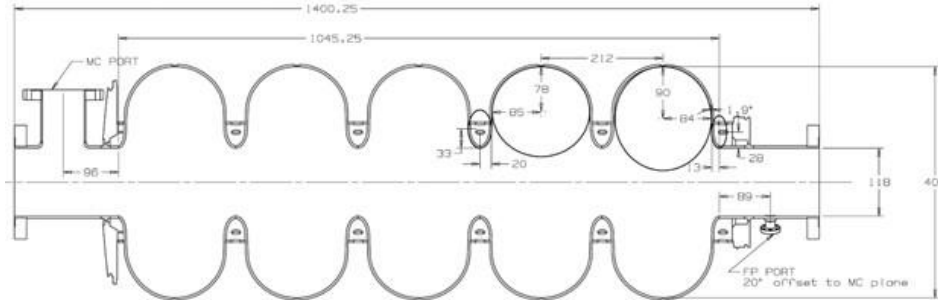


**FIGURE 8.** Drawing of the HB650 cavity.

The cavity is built from 4 mm thick high RRR niobium sheet material via stamping and electron beam welding (EBW). Vacuum seals on all demountable interfaces are achieved via NbTi flanges using AlMg diamond seal gaskets. The cavity is stiffened with 100 mm inner diameter high RRR 4 mm thick niobium stiffening rings. NbTi transition spools, which are stiffened by the same rings, provide the interface to the helium vessel and cavity tuner. The transition spools are EB welded to the beam tubes on each end group. Grade 2 titanium end cans, bellows, and helium vessel, which are TIG welded to the transition rings and to each other, form the liquid helium enclosure. A cylindrical helium vessel will be furnished with two helium inlets for fast cavity cooling, with a chimney to remove up to 33 W of average dissipated power as well as positioning and tuner lugs.

All auxiliary components and the cryomodule are identical to the PIP-II HB650 cryomodule shown in Figs. 6 and 9. The HB650 cryomodule can operate in either CW or pulsed mode.

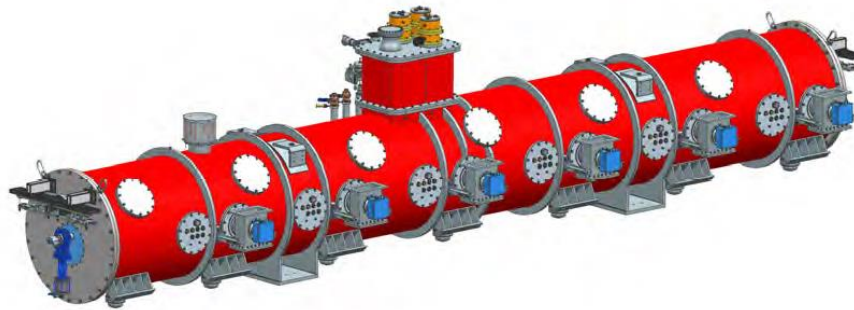


**FIGURE 9.** HB650 cryomodule.

The BRL 2.4 → 8 GeV Linac design is based on the LCLS-II/LCLS-II-HE cryomodule design (Fig. 7) [8]. As this design is based on XFEL/ILC cryomodules, it is capable to operate in either CW or pulsed mode. Table 4 lists the Linac parameters for pulsed mode of operation. Here we assume that with further R&D progress, the 9-cell SRF cavities will be able to operate at 35.5 MV/m at  $Q_0 = 2 \times 10^{10}$  (compared to the ILC baseline of 31.5 MV/m at  $1 \times 10^{10}$ ).

## H- LINAC CONSTRAINTS: BEAM LOSSES

Beam losses can be a significant limitation in a high intensity Linac. To keep the radio activation of the beam line components low enough for “hands-on maintenance”, activation levels must be below ~100 mrem/hr at 30 cm from a component surface, after extended operation. From previous experience this implies losses of less than ~1 W/m. A safety limit of ~0.2 W/m would allow relatively unrestricted maintenance [9, 10].

### Magnetic stripping constraints

The 8 GeV Linac beam must be transmitted as  $H^-$ , for compatibility with  $H^-$  injection into the Recycler or Main Injector, and the bending fields in the 8 GeV BRL transports are limited to  $\sim 0.06$  T to avoid magnetic stripping to  $H^0$  [11]. The 8 GeV Linac has three locations with significant amounts of bending magnets: the initial bend of  $\sim 45^\circ$  following the PIP-II Linac where the beam has an energy of  $\sim 1$  GeV, the bend of  $\sim 105^\circ$  at the end of the 3 GeV CW Linac, and smaller bends at 8 GeV associated with injection into the Recycler/Main Injector.

The stripping length can be estimated using this formula of Schrek [12]:

$$L_{strip} = \beta\gamma c \tau = \beta\gamma c \frac{a}{3.197 B_t p} \exp\left(\frac{b}{3.197 B_t p}\right) \quad \text{meters,}$$

where  $p$  is the  $H^-$  momentum,  $B_t$  is the magnetic field and  $a$  and  $b$  are parameters fitted from data. Keating et al. [13] obtained  $a = 3.073 \cdot 10^{-14}$  and  $b = 44.14$  from 800 MeV data.

For 1 GeV protons the transport is a mirror image of the PIP-II transport to the Booster. For that transport, the PIP-II design set a limit of 0.277 T, at which  $\tau = 0.12$  s, and  $L = 6.43 \cdot 10^7$ . Losses per meter would be  $1.6 \cdot 10^{-8}$ , which would be 0.032 W/m at 2MW beam power. The  $60^\circ$  requires  $\sim 21.4$  m of bend, which must be included in an achromatic lattice. The total losses would be  $\sim 3.5 \cdot 10^{-7}$ , which is relatively small.

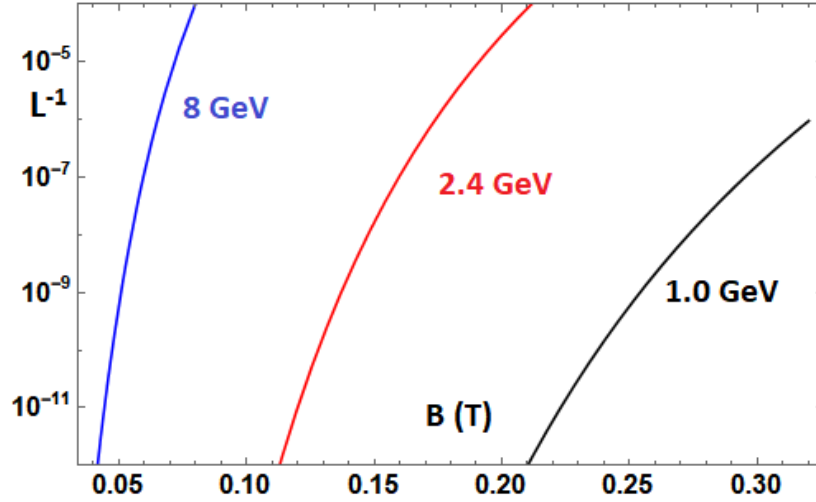


**FIGURE 10:** Magnetic stripping rate ( $m^{-1}$ ) as a function of  $B$  (T) for 1, 2.4 and 8 GeV  $H^-$ . Requiring  $L^{-1} \sim 10^{-8}$  requires  $B \cong 0.27, 0.15, 0.055$  T for  $E_{H^-} = 1, 2.4, 8$  GeV, respectively.

### Electron Stripping

A related question is whether the  $H^-$  ions could be stripped by the acceleration cavity fields, and whether that sets a limit on the cavity maximum field that is lower than other gradient limits. In a periodic acceleration structure having large aperture and a phase velocity  $\beta = 1$ , the axial electric field distribution on the axis is close to sinusoidal. This means that the maximal longitudinal electric  $E_z(z)$  field on the axis is two times higher than the acceleration gradient  $E_{acc}$ :

$$E_{x,max} = 2 E_{acc}.$$

According to Maxwell equations, in the paraxial area the RF magnetic field has only an azimuthal component, which is equal to

$$B_\phi(r, z) = -\frac{i\omega r}{c^2} E_z(z);$$

where  $\omega$  is the RF circular frequency, and  $c$  is speed of light. The maximal magnetic field amplitude is

$$B_{\phi, \max}(r, z) = \frac{\omega}{c^2} \frac{r}{2} E_{z, \max} = \frac{r\omega}{c^2} E_{acc}.$$

There is no stripping caused by the RF magnetic field if

$$B_{\phi, \max}(r, z) = \frac{r\omega}{c^2} E_{acc} \leq B_0 = 0.056 T.$$

Therefore, the acceleration gradient limitation is:

$$E_{acc} < \frac{c^2}{r\omega} B_0 = \frac{\lambda}{2\pi r} c B_0,$$

where  $\lambda$  is the RF wavelength.

The stripping rate for  $H^-$  as a function of electric field is shown in Fig. 10.

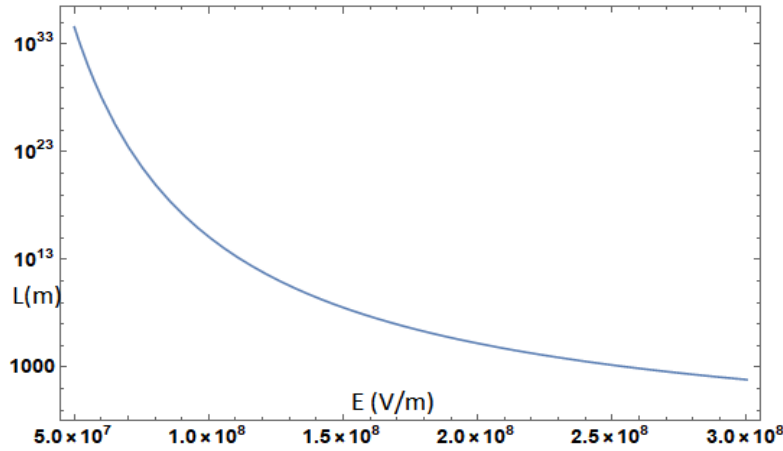


**FIGURE 10:** Stripping length as a function of electric field for 8 GeV  $H^-$ . At 50 MV/m the mean stripping length is greater than  $10^{34}$  m. This is reduced to  $3.5 \times 10^8$  m at  $E = 150$  MV/m.

In the beam frame the magnetic field transforms into an electric field with a magnitude of  $\beta\gamma c B_\phi$ . The rms beam emittance is  $\sim 0.3$  mm-mrad (normalized), which places the 8 GeV rms beam size at  $\sim 1$  mm, at a large  $\beta_L = 30$  m. If the beam particles have amplitudes less than  $\sim 1$  cm, the 0.056 T limit on transverse magnetic field used in the bending magnets transforms to a limit of  $\sim 60$  MeV/m. Provided that particle amplitudes can be confined within  $< \sim 1$  cm, magnetic and electric field stripping in the SRF cavities should not be a significant problem, particularly if  $E_{acc}$  is less than  $\sim 40$  MV/m.

### Intra-beam Scattering

An unexpected beam loss mechanism in the  $H^-$  Linac at SNS was identified by Lebedev as due to neutralization from intra-beam stripping. The PIP-III Linac is also  $H^-$  and is therefore vulnerable to this loss mechanism. An equation for the beam loss due to intra-beam stripping is presented in [14]:

$$\frac{1}{N} \frac{dN}{dt} = \frac{N \sigma_{\max} \sqrt{\sigma_{vx}^2 + \sigma_{vy}^2 + \sigma_{vz}^2}}{8\pi^2 \sigma_x \sigma_y \sigma_z} F(\sigma_{vx}, \sigma_{vy}, \sigma_{vz})$$

where  $\sigma_{max} \approx 4 \times 10^{-15} \text{ cm}^{-2}$ ,  $N$  is the number of  $\text{H}^-$  ions/bunch,  $\sigma_x$ ,  $\sigma_y$ ,  $\sigma_z$  are beam sizes in the beam frame,  $\sigma_{vx}$ ,  $\sigma_{vy}$ ,  $\sigma_{vz}$  are beam velocity spreads and

$$F(a,b,c) = \frac{1}{\pi} \int_{-\infty}^{\infty} \sqrt{\frac{x^2}{a^2} + \frac{y^2}{b^2} + \frac{z^2}{c^2}} e^{-\frac{x^2}{a^2} - \frac{y^2}{b^2} - \frac{z^2}{c^2}} \frac{dx dy dz}{abc}.$$

$N$  is  $\sim 1.9 \times 10^8$  at 5 mA peak current,  $\sigma_x = (\epsilon_{n,x} \beta_x / \beta \gamma)^{1/2}$ ,  $\theta_{x,rms} = (\epsilon_{n,x} / \beta_x / \beta \gamma)^{1/2}$ ,  $\theta_{\mu,rms} = \delta p / p$  and  $\sigma_s$  is the bunch length. The integrated function  $F$  is close to 1 at Project X parameters. At typical parameters ( $\epsilon_n = 0.3 \times 10^{-6}$  m-rad,  $\beta_{x,y} = 10$  m,  $\gamma = 2.07$  to  $9.53$  ( $1 \rightarrow 8$  GeV),  $\sigma_s = 1.5$  mm,  $\theta_{\mu} \approx 0.0003$ ),  $dN/ds/N$  is  $\sim 4 \times 10^{-8}/\text{m}$  (1 GeV) to  $\sim 2 \times 10^{-8}/\text{m}$  (8 GeV). This would correspond to 0.04 to 0.02 W/m at 1 MW. A more complete evaluation of these was made by Ostiguy for Project X, with evaluation of beam sizes from tracking through the lattice [15]. Those results were similar to the present evaluation.

### Black-body radiation stripping

The beam pipe would be filled with low-energy photons from thermal black body radiation. At room temperature (300 K),  $kT = 0.02587$  eV and the spectral energy distribution peaks at  $\sim 0.06$  eV. A much larger exchange of  $E_0 = 0.754$  eV is needed to ionize  $\text{H}^-$  at rest. The photons are Doppler shifted by a factor of up to  $2\gamma$  in the  $\text{H}^-$  ion rest frame at high energies. At 8 GeV, the peak is shifted above that threshold and  $\text{H}^-$  stripping can occur [9].

The photodetachment cross section is:

$$\sigma(E') = 8\sigma_{max} \frac{E_0^{3/2} (E' - E_0)^{3/2}}{E'^3},$$

where  $\sigma_{max} = 4.2 \times 10^{-21}$  and  $E'$  is the photon energy in the  $\text{H}^-$  rest frame:

$$E' = \gamma(1 + \beta \cos \alpha)E.$$

The stripping rate can be calculated using the following equation:

$$\frac{1}{L} = \frac{8\sigma_{max} E_0^{3/2}}{2\pi^2 \beta \gamma^3 (\hbar c)^3} \int_{E_0}^{\infty} dE' \int_{-1}^{+1} du \frac{1}{(1 + \beta u)^2} \frac{(E' - E_0)^{3/2}}{E'} \frac{1}{[\exp(E' / kT \gamma(1 + \beta u)) - 1]}.$$

We evaluated this expression to be  $\sim 7.8 \times 10^{-7} / \text{m}$ , in good agreement with Carneiro, et al. [8]. This is a fairly large value. The pulsed version of the 8 GeV beam ( $\sim 200$  kW) would have 0.16 W/m while a CW version at 2 MW would have 1.56 W/m. The transport at 8 GeV is relatively short, so the resulting beam loss should be manageable ( $1.56 \times 10^{-5}$  in 20 m). The radiation stripping can be greatly reduced by cooling the beam pipe to a lower temperature, which reduces the photon energy spectrum proportionately. A reduction to 150 K (from liquid nitrogen cooling) would reduce losses to  $\sim 2.5 \times 10^{-8}$ , enabling easier maintenance and more manageable CW operation.

### Beam-gas stripping

Collisions of  $\text{H}^-$  with background gas molecules can strip the  $\text{H}^-$  ions, causing beam loss [9]. The lifetime  $\tau_m$  of an  $\text{H}^-$  ion in the presence of residual gas is given by:

$$\tau_m = \frac{1}{\beta c d_m \sigma_m},$$

where  $d_m$  is the gas particle density and  $\sigma_m$  is the interaction cross section. The beam fraction loss per unit length is:

$$\frac{1}{L} = \frac{1}{\tau_m \beta c}.$$

This is to be summed over gas components. If we assume the gas is "air", then  $\sigma_m = \sim 0.65 \times 10^{-18} \text{ cm}^2$  and  $d_m = 3.2 \times 10^{22} P$  (torr) m at  $T = 300$  K then  $L^{-1} = 2.1 P$  (torr)  $\text{m}^{-1}$ . With a vacuum of  $10^{-8}$  Torr, losses are  $2.1 \times 10^{-8} / \text{m}$ . or 0.042 W/m

for a 2 MW beam. [12] used a generic vacuum of 70% H<sub>2</sub>, 10% H<sub>2</sub>O, 10% CO<sub>2</sub>, 10% CO), which would make the average value of  $\sigma_m \sim 0.15 \times 10^{-18}$  and reduce the losses by a factor of  $\sim 4$  at the listed pressure.

### MI/RR INJECTION

The locations of PIP-II and the Main Injector, as well as the requirement that MI extraction feed the LBNF beamline, restrict the possible locations for H<sup>-</sup> injection. Charge exchange injection requires modification of a long straight section. MI-10 is the only long straight section that readily accommodates a Linac from PIP-II to the MI. The next possibility, MI-30, is another km downstream, and requires extra bending which would strip H<sup>-</sup> ions. The previous straight section, MI-60, would either inject into the MI in the wrong direction or require a  $\sim 180^\circ$  bend that would strip H<sup>-</sup> ions. However, MI-10 has been chosen as the straight section for extraction to LBNF, and the extraction kickers and septum magnets will occupy the space needed for injection to the MI. Unless MI extraction is changed, MI-10 cannot be used for charge exchange injection.

The Recycler Ring lies directly above the MI, and its corresponding straight section, RR-10 can be modified to accommodate charge exchange injection. The recycler ring can then be used to accumulate multiple pulses from the Linac to be followed by single turn transfer to the MI at MI-22 or MI-30. That general injection procedure was included in the Project X plan and was developed in some detail by D. Johnson et al. [10] and A. Drozhdin et al. [16]. That injection is the baseline injection plan considered in this report, modified to match the present MI conditions.

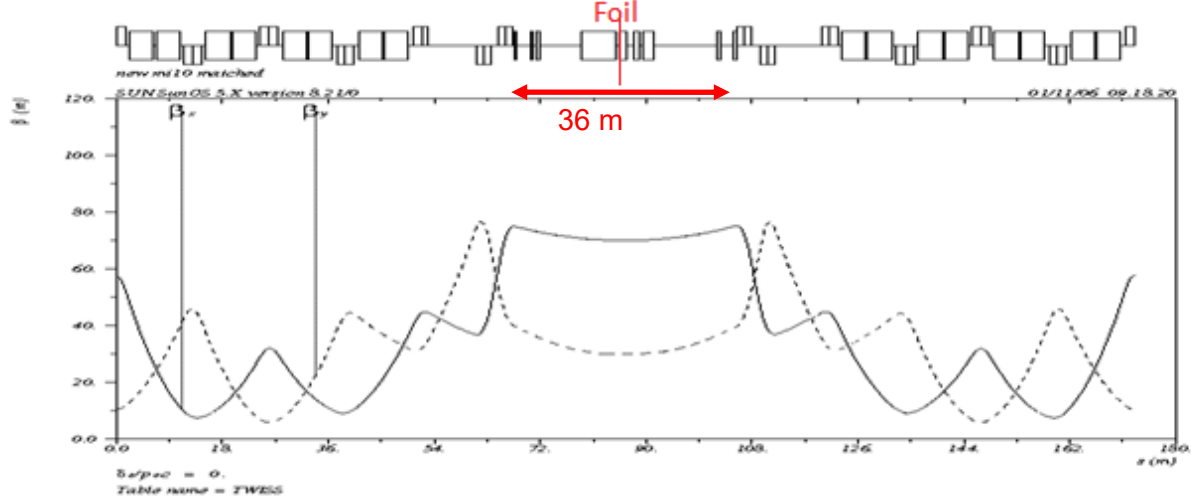


**FIGURE 11.** Lattice with betatron functions for the RR-10 straight section, adapted for foil injection. A  $\sim 36$  m segment between focusing quads is reserved for injection kickers, injection bump magnets and stripping foil.

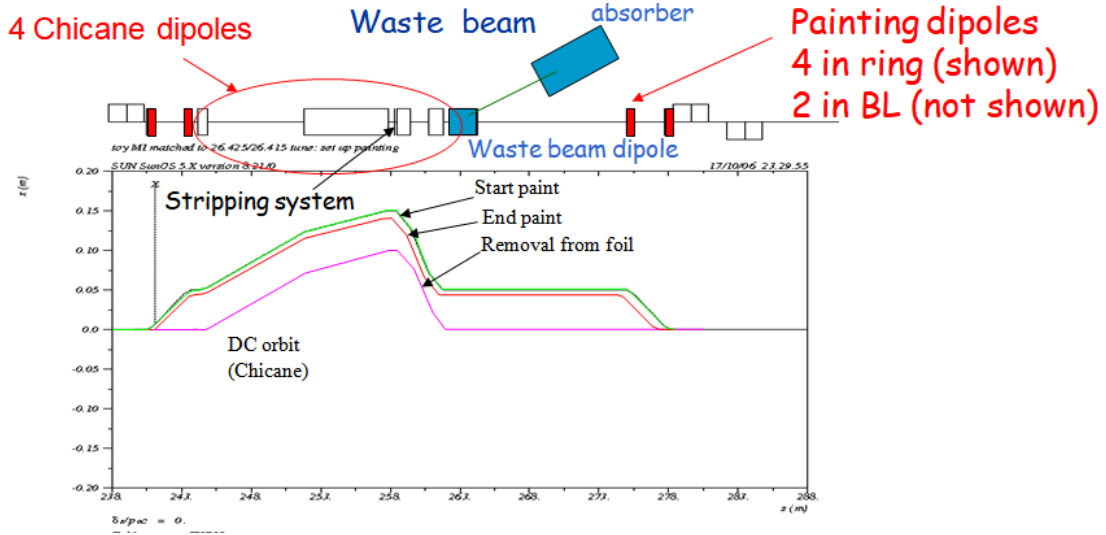


**FIGURE 12.** Injection insert components with kickers, and orbit variations used for injection with painting on the foil.

### Foil injection

The baseline injection method from the Linac into the RR is multiturn foil-stripping injection. During injection the beam orbit is displaced toward the foil by a 4-dipole chicane (see Fig. 12). The long second dipole (with a low field of  $B = 0.055\text{T}$ ) is shared by both circulating beam ( $\text{H}^+$  or protons) and the injected  $\text{H}^-$  beam to converge on the foil between the middle dipoles. The smaller  $\text{H}^-$  beam strikes the foil in a corner of the circulating proton beam distribution, where the  $\text{H}^-$  ions are stripped to  $\text{H}^+$  to join the circulating beam distribution. The painting dipole fields are varied such that the injected  $\text{H}^+$  populate the circulating distribution matched to the enlarged final beam emittance, while minimizing the number of foil hits per proton.

High intensity multiturn  $\text{H}^-$  injection into the RR/MI, with injection painting and foil heating, was simulated by Drozhdin et al. [16] and further explored by Neuffer [17]. Injection requires  $\sim 26\text{ mA}\cdot\text{ms}$  of beam. At  $1 - 2\text{ mA}$ , this implies  $2300 - 1150$  turns. If this were injected in a single pulse, the foil would heat to  $\sim 2500\text{ K}$ , which is unacceptably high. (Unacceptable sublimation would occur at  $\sim 1800\text{ K}$ .) The preferred injection procedure is to split the injection into a number of separate shorter injections, spaced by the pulsed Linac rep rate, and then sequentially inject into the ring, while following a foil painting program to minimize the number of foil hits. Fig. 13 displays calculations of foil heating in a 6-step injection at  $1, 2, 4\text{ mA}$  currents, which reduces peak  $T$  to  $2200, 1660,$  and  $1250\text{ K}$ , respectively. The  $2$  and  $4\text{ mA}$  numbers are acceptable. Parameters of injection scenarios are presented in Table 6.

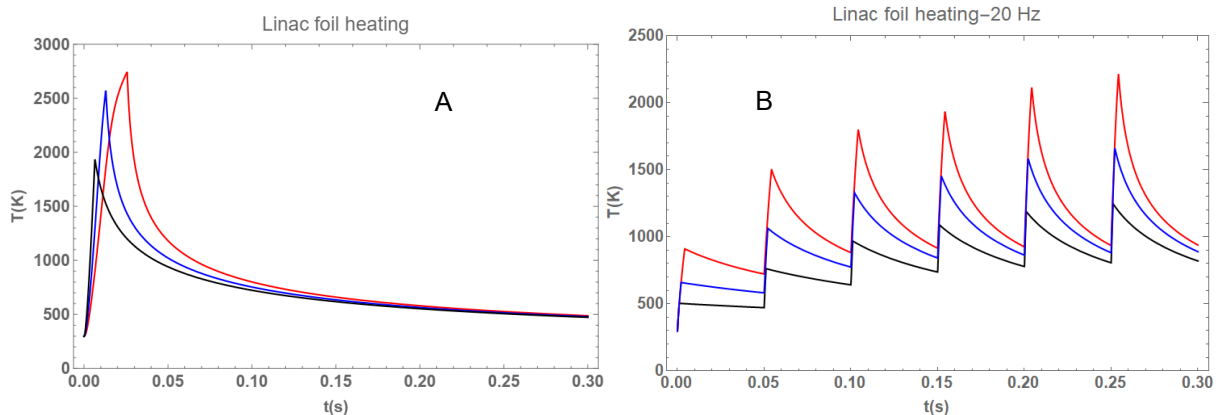


**FIGURE 13.** A) Foil heating with single  $26\text{ mA}\cdot\text{ms}$  injection at  $1\text{ mA}$  (red),  $2\text{ mA}$  (blue) and  $4\text{ mA}$  (black). B) Foil heating in 6-step injection ( $4.4\text{ mA}\cdot\text{ms}/\text{step}$ ) at  $1\text{ mA}$  (red),  $2\text{ mA}$  (blue) and  $4\text{ mA}$  (black).

**Table 6:** Summary of injection scenario parameters. In the first three cases the RR is filled with a single long pulse of 1 mA, 2 mA, and 4 mA, respectively. In the last three injection is split into 6 separate (20 Hz) pulses.

Scenario	1 mA-26 ms	2 mA	4 mA	6 1 mA-4.3 ms	2 mA	4 mA
Injection time	25.72 ms	14.8	6.9	6×4.28 ms	6×2.2 ms	6×1.1 ms
Number of turns	2334	1167	584	6×395	6×198	6×99
Ave hits/proton	120	61	33	120	60	32
Max hit density	$5.15 \times 10^{14}$	$2.60 \times 10^{14}$	$1.33 \times 10^{14}$	$5.14 \times 10^{14}$	$2.58 \times 10^{14}$	$1.31 \times 10^{14}$
Maximum foil $T$	2750 K	2580 K	1930 K	2215 K	1660 K	1250 K

### Beam Losses at injection

In  $H^-$  injection the beam passes through a foil, where interactions with the foil material causes the ion to lose electrons, eventually being stripped to  $H^+$  (protons) that can be stored and accelerated. The  $H^-$  ions are stripped to  $H^0$  and  $H^+$ , and  $H^0$  ions are stripped to  $H^+$ . Equations for stripping versus foil thickness have been developed by Gulley et al. [18], from fits to measured stripping data. The equations are [19]:

$$f_{H^-}(t, \beta) = \text{Exp}[-(0.479 + 0.0085) \cdot 0.05t / \beta^2] ,$$

$$f_{H^0}(t, \beta) = \frac{0.479}{(0.479 + 0.0085 - 0.187)} \left( \text{Exp}[-(0.187) \cdot 0.05t / \beta^2] - \text{Exp}[-(0.479) \cdot 0.05t / \beta^2] \right) ,$$

$$f_{H^+}(t, \beta) = 1 - f_{H^0}(t, \beta) - f_{H^-}(t, \beta) ,$$

where  $\beta = v/c$  is the usual kinematic factor for the incident  $H^-$ ,  $t$  is the carbon foil thickness in  $\mu\text{g}/\text{cm}^2$ . For a  $500 \mu\text{g}/\text{cm}^2$  thick foil, 98.6% of initial  $H^-$  are stripped to  $H^+$  (protons). For graphite (at density  $\rho = 2.0 \text{ g}/\text{cm}^3$ ), this is a  $2.5 \mu\text{m}$  thick foil, or  $1.4 \mu\text{m}$  thick for diamond ( $\rho = 3.6$ ). Fig. 14 shows the variation of ion fraction through a foil with thickness of  $500 \mu\text{g}/\text{cm}^2$ , which will be our reference design thickness.

Unstripped ions ( $H^-$  and  $H^0$ ), including injected beam that misses the foil, are magnetically separated from the circulating beam in the dipole just downstream of the foil with the  $H^-$  ions, stripped by a thicker downstream foil and directed into a beam absorber, designed to localize losses in a shielded enclosure. This enclosure and absorber will require new construction downstream of RR-10, and it will be constrained by the proximity of MI extraction beam and the MI and RR rings. From previous designs, we expect  $\sim 2\%$  of the incoming beam to be lost, with  $\sim 90\%$  of that captured into the absorber;  $\sim 0.2\%$  will be lost in a relatively uncontrolled manner in the near vicinity of extraction or further downstream in the RR. Future detailed design effort must determine that these losses are adequate managed.

The injected beam and the accumulating proton beam will pass through the foil, losing energy and scattering, with energy straggling. This can lead to beam losses from rms emittance growth and large angle scattering events.

Table 7 summarizes the various loss mechanisms, expected losses, and mitigation strategies for the BRL, including Linac and injection losses.

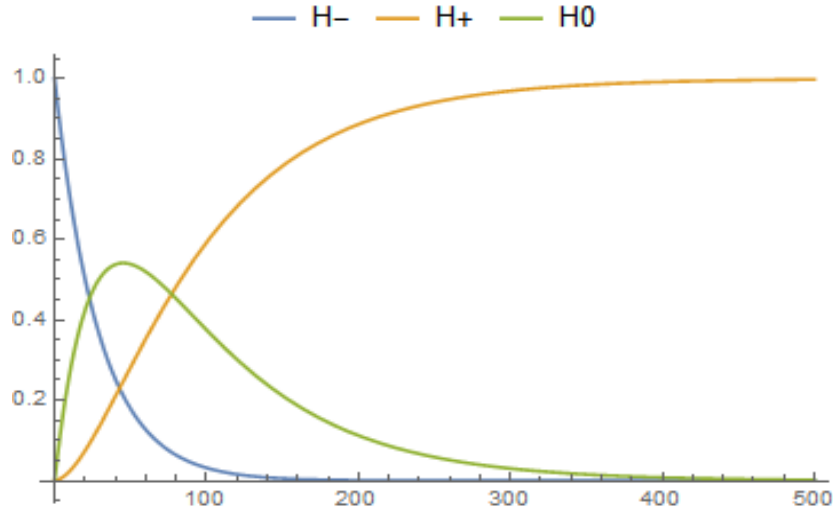


**FIGURE 14.** Fraction of beam that is  $H^-$ ,  $H^0$ , or  $H^+$  as it passes through a C foil with final thickness of  $500 \mu\text{g}/\text{cm}^2$ . At  $400 \mu\text{g}/\text{cm}^2$ , the beam is  $\sim 96.4\%$   $H^+$ , and  $3.6\%$   $H^0$ . At  $500 \mu\text{g}/\text{cm}^2$ , it is  $\sim 98.6\%$   $H^+$ . At  $600 \mu\text{g}/\text{cm}^2$ , it would be  $\sim 99.5\%$   $H^+$ .

**Table 7:** Loss mechanisms, expected effects and mitigation.

Loss process	Key parameters	Loss per meter	Estimated Losses	Mitigation Strategies
Magnetic stripping	$B(1 \text{ GeV}) < 0.28\text{T}$ $B(2.4 \text{ GeV}) < 0.15\text{T}$ $B(8 \text{ GeV}) < 0.055\text{T}$	$1.6 \times 10^{-8}$ $2 \times 10^{-8}$ $10^{-8}$	$3 \times 10^{-7}$ $3 \times 10^{-6}$ $10^{-7}$	Limiting $B$ -fields
Black-body Radiation	1 GeV 2.4 GeV 8 GeV $T = 300 \text{ K}$	$3.7 \times 10^{-8}$ $1.0 \times 10^{-7}$ $7.8 \times 10^{-7}$	$10^{-6}$ $1.6 \times 10^{-5}$ $\sim 10^{-6}$	Shorter, shielded transport Cooled beam pipe
Beam-gas interactions	$P \sim 10^{-8} \text{ Torr}$	$2.1 \times 10^{-8}$	$< \sim 10^{-5}$	Vacuum
Intrabeam stripping	$N = 2 \times 10^8 / \text{bunch}$	$2 - 4 \times 10^{-8}$	$< \sim 10^{-5}$	Short transports
Foil –beam misses	$500 \mu\text{g}/\text{cm}^2 \text{ C foil}$		$\sim 2\%$	Collimation before foil, matching, absorber
Foil- $H^0$			$\sim 1\%$	Injection absorber
Foil-large-angle scattering	$40\pi \text{ mm-mrad}$ acceptance		400 W	Collimation, reduce foil crossings
Foil-nuclear interaction	$L_N = 60 - 86 \text{ gm}/\text{cm}^2$		60 W	Collimation, shielding

### Variant injection scenario

The recycler-based RR-10 injection provides the most direct injection from the BRL into the MI tunnel, but is limited by the restricted geometry of the MI-10 region, and requires accumulation in the recycler ring and transfer to the MI. The use of the Recycler also fixes the injection energy at 8 GeV. A direct injection into the MI would enable full use of the larger MI aperture and could accommodate different injection energies and could simplify the injection scenario. Direct injection into MI-10 is not possible without changing MI extraction, and other MI straight sections are not readily available for injection from the BRL.

An alternative injection scenario is displayed in Fig. 15. The Linac is reconfigured to inject into a new  $\sim 8 \text{ GeV}$  storage ring, which is placed inside the Main Ring near MI-60. The new ring would be designed with an acceptance larger than the MI, would have an injection straight optimized for multiturn foil injection from the Linac and an extraction matched into the Recycler or MI at MI-60 or MI-62. The ring is  $\sim 1/6$  of the MI in circumference; 6 boxcar stacked pulses from the ring would fill the RR or MI in each MI cycle.

This scenario requires the construction of a new storage ring, which can have an injection system fully optimized to limit and control losses. In cycles not needed for MI-DUNE, the storage ring could also accumulate 8 GeV beam

for other experiments, including neutrino beams, pulsed pion and muon beams. The stored beam may also be needed for the Fermilab high-intensity program that will complement the DUNE-based High-energy neutrino program.

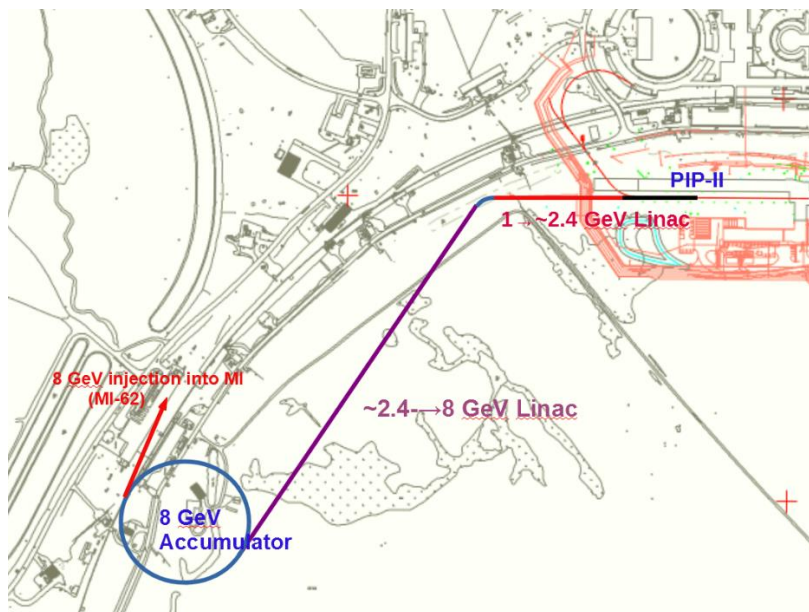


**FIGURE 15:** Alternative layout of linac-based BRL. An 8 GeV Linac leads to an accumulator (~1/6 MI circumference), where foil stripping of  $H^-$  beam over 4.2 ms-mA pulses can occur.

## R&D REQUIREMENTS

The Booster Replacement program will require a significant R&D program to obtain a timely implementation of the required upgrade. The DOE project process requires detailed designs and evaluations of the proposal and alternatives, which implies both RCS and Linac-based approaches should be evaluated and compared.

The SRF is based on PIP-II cryomodules for the 650 MHz section and ILC/LCLS-II for the 1300 MHz Linac. The designs should be updated to incorporate recent improvements in SRF and optimized for cost and efficiency.

Other R&D topics that need to be investigated include:

- Simulation and modelling of the complete Linac design, from PIP-II into the MI.
- Simulation and optimization of the injection painting and foil heating.
- Consideration of laser-assisted injection and its adaptation to the BRL and RCS scenarios.
- An evaluation of SRF power and wall-plug power requirements for the scenarios, for pulsed and CW operation options, including optimizations, should be developed.
- An alternative injection into a new ~8 GeV storage ring could be considered; this would avoid the MI-10 bottleneck, but at the cost of an additional storage ring. The ring may be needed for intensity frontier experiments.

Some details of the proposed R&D program are outlined below.

### SRF research topics

Here is a list of key R&D topics that will be part of the BRL R&D program:

- 650 MHz: higher  $Q$  ( $>6 \times 10^{10}$ ) at 2 K and 23 MV/m – using nitrogen doping recipe improvement.
- 1300 MHz: high  $Q$  ( $>2 \times 10^{10}$ ) at 2 K and higher gradient of  $>35.5$  MV/m – using a new 2-step low T bake or some other recipe.
- Resonance control R&D for microphonics suppression (CW) and LFD compensation (pulsed).

- Ferroelectric tuner for both resonance control and coupling adjustment – will improve efficiency of the SRF systems.
- Robotic assembly of the SRF cavity strings in clean rooms – essential for achieving high gradients.

Most of these R&D topics are in line with the *DOE HEP General Accelerator R&D RF Research Roadmap* [23].

**Improving the 650 MHz cavity performance.** Recent progress in SRF experimental and theoretical research resulted in a dramatic increase in achievable quality factors by a) the development of new surface treatments resulting in very high-Q via nitrogen doping [24]; and b) achievement of very high Q under real accelerator conditions via efficient magnetic flux expulsion (fast cooling and low flux pinning) [25-26]. These advances have been confirmed at laboratories worldwide and transferred to industry. They have found practical demonstration in the LCLS-II cryomodules that have reached two times the previous state of the art Q on an accelerator scale unit with an average of  $Q \sim 3 \cdot 10^{10}$  at 2 K, 1.3 GHz, 16 MV/m [27]. Further improvement of the nitrogen doping recipe allows the LCLS-II-HE project to increase the accelerating gradient to 20.8 MV/m while maintaining the high quality factor. PIP-II has adapted nitrogen doping to their 5-cell 650 MHz elliptical cavities, with HB650 cavities ( $\beta_G = 0.92$ ) operating at 18.8 MV/m with  $Q > 3 \cdot 10^{10}$  [28]. Fig. 16 shows results of testing four cavities in the vertical test cryostat.

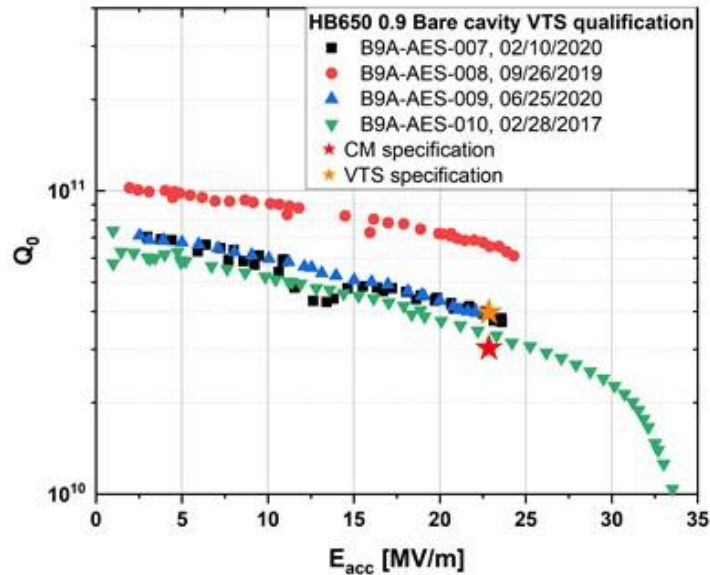


FIGURE 16: Vertical acceptance test of HB650  $\beta_G = 0.9$  cavities [25].

There are still ample R&D opportunities for improving the quality factor of 650 MHz SRF cavities to achieve the parameters desired for the BRL: 22.6 MV/m with  $Q > 6 \cdot 10^{10}$ . As we can see in Fig. 16, obtaining the gradient is already within reach. However, dedicated R&D on improving the nitrogen doping recipe will be needed to reliably achieve this quality factor.

**High gradient/ high Q R&D at 1300 MHz.** For the 1300 MHz pulsed linac, we will need a surface treatment recipe that would reliably produce cavities with the accelerating gradient of 35.5 MV/m and  $Q > 2 \cdot 10^{10}$ . Recently, as part of the ILC cost reduction R&D, a new treatment has been developed that combines ultra-cold electropolishing and a two-step low temperature bake [29]. Cavities treated with this recipe systematically achieve extremely high gradients of  $\sim 48$ -50 MV/m but at lower Q than we require for the BRL, see Fig. 17. Further studies must be performed to optimize the new recipe for BRL needs.

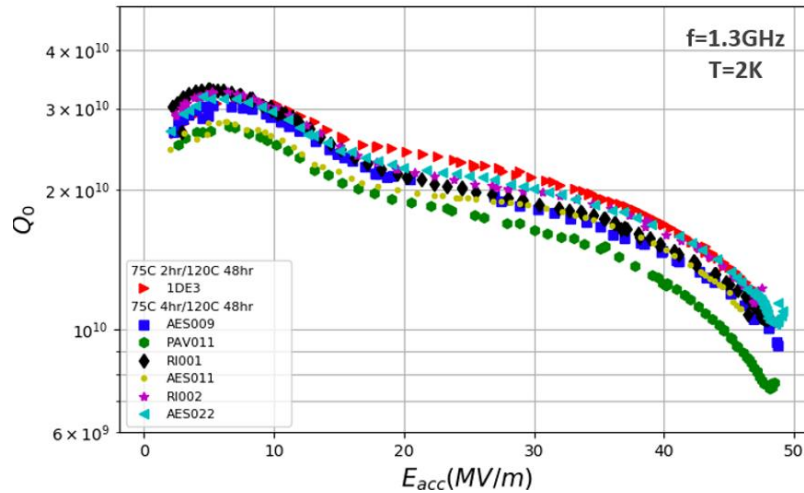
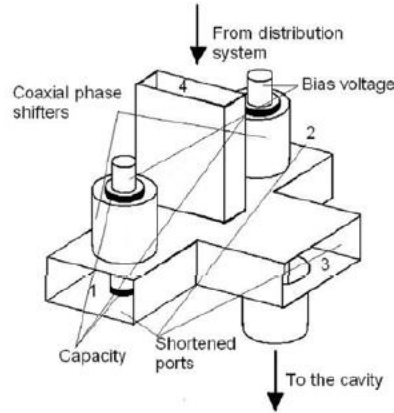


FIGURE 17: Vertical tests of single cell TESLA cavities treated with the new recipe.

**Resonance control of SRF cavities.** R&D for high acceleration gradient and high-Q should be supported by the cavity resonance control R&D [30-31]. SRF structures operating in the CW regime, like the 650 MHz linac for BRL, are susceptible to vibrations due to external excitation (microphonics). For pulsed-beam accelerators such as the 1300 MHz pulsed linac for BRL, compensating cavity resonant frequency detuning due to the Lorentz force (Lorentz Force Detuning or LFD) is especially important as the ratio of LFD over the cavity bandwidth is proportional to the cube of acceleration gradient. The sources of microphonics should be determined, understood, and mitigated. A robust active LFD with microphonics compensation algorithms should be developed for the BRL. The algorithm development shall be done in conjunction with developing fast cavity frequency tuners, based on either the currently dominant piezo-electric mechanical tuner technology or on a new ferroelectric technology described below.

**Ferroelectric tuner R&D.** Recently developed ferroelectric ceramics with low losses at RF frequencies [32-34] allow development of electrically controlled tuners with switching times much better than that of piezo-electric mechanical tuners. Such a tuner is inserted into a high-power transmission line connected to the SRF cavity and allows alteration of coupling between the acceleration structure and the line during the RF pulse [35]. In addition, this tuner would allow electronic control of cavity frequency by a device operating at room temperature within timescales of active compensation of microphonics. So, the ferroelectric tuner can perform the double function of coupling and frequency tuning. It would reduce cryogenic losses in the structure and consequently significantly reduce the overall energy consumption of the accelerator and could eliminate the need to use over-coupled fundamental power couplers, thus significantly reducing RF amplifier power. A proof-of-principle demonstration of the ferroelectric fast reactive tuner (FE-FRT) was successfully conducted at CERN [36]. The timescale in which the FE-FRT is able to shift the cavity frequency across the entire tuning range was measured to be  $< 50 \mu\text{s}$ , this is significantly faster than any other cavity tuning device. This measurement was limited by the signal to noise ratio and the true timescale could well be more than an order of magnitude lower still. This experiment paves a way toward developing a device that can produce fast cavity coupling change, such as shown in Fig. 18. More R&D efforts are needed in this area to fully realize the full potential of ferroelectric devices.



**FIGURE 18:** Schematic of a device to produce fast cavity coupling changes based on a magic-T and two phase shifters containing ferroelectric elements. This device is not under vacuum and is located outside of the cryostat [35].

**Robotic assembly of SRF cavity strings.** Field emission phenomenon could be a serious impediment to achieving high gradients. Special studies will be required in parallel with high gradient research for the BRL to abate field emission in vertical tests and cryomodules. One of the promising pathways is robotic assembly of SRF cavities in clean rooms. Using robots for automated assembly would eliminate cavity contamination and assembly inconsistencies due to the “human factor”, which is the dominant cause of the cavity performance degradation. This is a nascent R&D area that is just starting to receive proper attention at various laboratories around the world.

### Laser assisted injection R&D

Foil heating and damage, as well as beam losses associated with foil-based injection, are a significant limitation on the performance of high-intensity  $H^-$  injected beams, including both the RCS and the Linac-based versions of the Booster Replacement. Research has demonstrated that laser-assisted injection can be used for a proton ring [37]. The 1 GeV proton energy of this demonstration required relatively difficult ultraviolet light, which limited the pulse length.

Laser assisted injection is considered to be the eventual preferred procedure for  $H^-$  injection, but the R&D needed for implementation has not yet been performed. Laser Stripping of high-energy hydrogen atoms is relatively easy,

because the laser light is Doppler-shifted to higher energy in the rest frame following  $\lambda_{PF} = \frac{\lambda_{Lab}}{\gamma(1 + \beta \cos(\theta))}$ ,

where  $\gamma = 9.526$  and  $\beta = 0.9945$  for 8 GeV protons, and  $\theta$  is the angle between the laser and particle beam, which should be nearly collinear ( $\theta \cong 0^\circ$ ). The laser intensity  $I_0$  in the lab frame is boosted in the beam frame to  $I_{BF} = I_0(1 + \beta \cos(\theta))^2 \gamma^2$ . Hydrogen ionization requires  $\sim 90$  nm photons, which can be obtained from Doppler-shifted  $\sim 1700$  nm laser light, and the intensity would be magnified by a factor of 360. A high intensity infrared (1000-1700 nm) laser matched to the proton injection pulse could be possible [38]. Figure 19 shows a simplified view of a possible stripping configuration. A redesign of the injection scenario to include laser injection should be developed, and compared to the baseline foil injection. This should be followed by the acquisition and testing of some of the

hardware needed for laser injection, possibly including a high-power laser. A beam test at Fermilab may be possible.

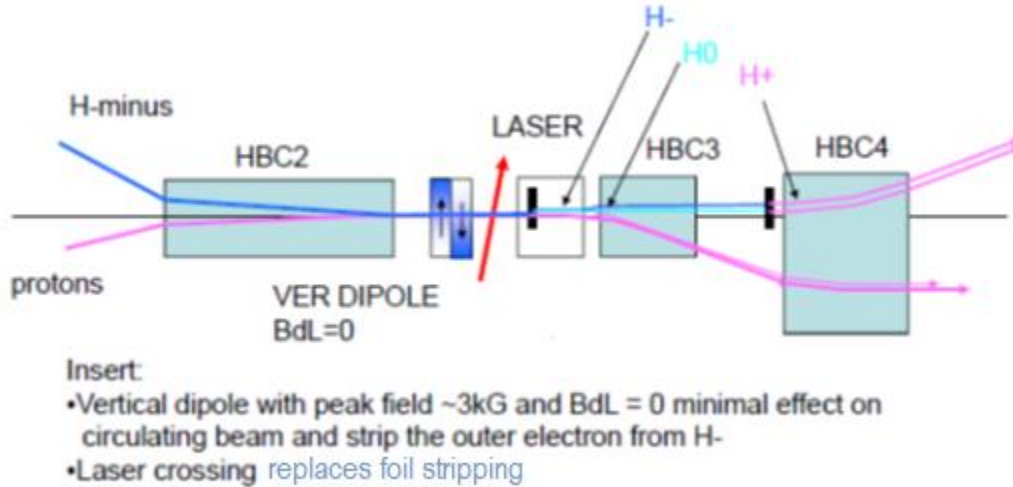


FIGURE 19: Schematic view of a laser-stripping injection system that could replace foil injection.

## ACKNOWLEDGMENTS

This manuscript has been authored by Fermi Research Alliance, LLC under Contract No. DE-AC02-07CH11359 with the U.S. Department of Energy, Office of Science, Office of High Energy Physics.

## References

1. M. Ball et al., *The PIP-II Conceptual Design Report* (2017).
2. *Project X Accelerator Reference Design, Physics Opportunities, Broader Impacts*, June 2013, Fermilab TM-2557.
3. S. Holmes, “Proton Improvement Plan II,” presentation at the Fermilab Users meeting, June 11, 2014. in
4. R. Ainsworth et al., “An Upgrade Path for the Fermilab Accelerator Complex”, TM-2754-AD-APC-PIP2-TD, Fermilab, Batavia IL, USA, 2021.
5. A. Grassellino et al., “Nitrogen and argon doping of niobium for superconducting radio frequency cavities: a pathway to highly efficient accelerating structures,” *Supercond. Sci. Technol.* **26**, 102001 (2013) (Rapid Communication).
6. A. Romanenko et al., “Dependence of the residual surface resistance of superconducting radio frequency cavities on the cooling dynamics around  $T_c$ ,” *J. Appl. Phys.* **115**, 184903 (2014).
7. D. Bafia et al., “Gradients of 50 MV/m in TESLA shaped cavities via modified low temperature bake,” *Proc. SRF2019*, Dresden, Germany, p. 586 (2019).
8. LCLS-II Design Team, *LCLS-II Final Design Report*, LCLSII-1.1-DR-0251-R0 (2019).
9. J. P. Carneiro, B. Mustapha and J. P. Ostroumov, “Numerical simulations of stripping effects in high intensity hydrogen ion linacs,” *Phys. Rev. STAB* **12**, 040102 (2009).
10. D. Johnson, “Conceptual Design Report of 8 GeV H- Transport and Injection for the Fermilab Proton Driver,” Beams-doc 2597 (2007).
11. W. Chou et al., “8 GeV H- ions: transport and injection,” *Proc. PAC2005*, Knoxville, TN, USA, p. 1222 (2005).
12. L.R. Scherk, , “An improved value for the electron affinity of the negative hydrogen ion”, *Canadian J. of Phys*, **57**, 558 (1979).
13. P.B. Keating et al., “Electric-field-induced electron detachment of 800-MeV ions” , *Phys. Rev. A* **52**, 4547 (1995).
14. V. Lebedev et al., “Intrabeam stripping in H- Linacs,” *Proc. LINAC2010*, Tsukuba, Japan, p. 929 (2010).
15. J.-F. Ostiguy, “Intrabeam Stripping,” Project-X Note 698 (2010).
16. A. I. Drozhdin, I. L. Rakhno, S. I. Striganov, and L. G. Vorobiev, “Modeling multiturn stripping injection and foil heating for high intensity proton drivers”, *Phys. Rev. STAB* **15**, 011002 (2012).
17. D. Neuffer, “Injection from 8 GeV PIP-III Linac to Main Injector,” FERMILAB-TM-2739-AD (2020).
18. M. S. Gulley et al., *Physical Review A* **53**, 3201-3210 (1996).

19. M. Plum, "Stripper Foils for H- Beams," in *Handbook of Accelerator Physics and Engineering*, second edition, A. W. Chou, K. H. Weiss, M. Tigner and F. Zimmermann, eds., p. 574, 2013.
20. N. Solyak, "Project-X CW Linac (ICD-2+) Lattice Design," Project X presentation, March 16, 2010.
21. *Long-Baseline Neutrino Experiment (LBNE) Project Conceptual Design Report Volume 2: The Beamline at the Near Site*, October 2012.
22. S. Nagaitsev, D. E. Johnson, and J. Lackey, "Project X: 8 GeV Recycler Injection," Project X doc. 74 (2007).
23. *Radiofrequency Accelerator R&D Strategy Report: DOE HEP General Accelerator R\&D RF Research Roadmap Workshop, March 8-9, 2017*, <https://doi.org/10.2172/1631119>
24. A. Grassellino et al., "Nitrogen and argon doping of niobium for superconducting radio frequency cavities: a pathway to highly efficient accelerating structures," *Supercond. Sci. Technol.* **26**, 102001 (2013) (Rapid Communication).
25. A. Romanenko et al., "Dependence of the residual surface resistance of superconducting radio frequency cavities on the cooling dynamics around  $T_c$ ," *J. Appl. Phys.* **115**, 184903 (2014).
26. A. Romanenko et al., "Ultra-high quality factors in superconducting niobium cavities in ambient magnetic fields up to 190 mG," *Appl. Phys. Lett.* **105**, 234103 (2014).
27. M. C. Ross, "LCLS-II status, issues and plans," *Proc. SRF2019*, Dresden, Germany, p. 1 (2019).
28. *Proton Improvement Plan-II: Final Design Report*, Fermilab (2021).
29. A. Grassellino et al., "Accelerating fields up to 49 MV/m in TESLA-shape superconducting RF niobium cavities via 75°C vacuum bake," <https://arxiv.org/abs/1806.09824>.
30. W. Schappert, "Resonance control for future linear accelerators," *Proc. LINAC2016*, East Lansing, MI, USA, p. 363 (2016).
31. Y. Pischalnikov et al., "Design and test of compact tuner for narrow bandwidth SRF cavities," *Proc IPAC2015*, Richmond, VA, USA, p. 3352 (2015).
32. E. Nenasheva et al., "Low loss microwave ferroelectric ceramics for high power tunable devices," *Journal of European Ceramic Society* **30**, 395 (2010). [doi:10.1016/j.jeurceramsoc.2009.04.008](https://doi.org/10.1016/j.jeurceramsoc.2009.04.008)
33. A. Kozyrev et al., "Observation of an anomalous correlation between permittivity and tunability of a doped (Ba,Sr)TiO<sub>3</sub> ferroelectric ceramic developed for microwave applications," *Appl. Phys. Lett.* **95**, 1 (2009). <http://doi.org/10.1063/1.3168650>
34. A. Kanareykin et al., "Observation of an Anomalous Tuning Range of a Doped BST Ferroelectric Material Developed for Accelerator Applications," *Proc. IPAC'10*, Kyoto, Japan, pp. 3987 (2010).
35. S. Kazakov et al., "Fast ferroelectric L-band tuner," *AIP Conference Proceedings* **877**, 331 (2006). <https://doi.org/10.1063/1.2409153>
36. N. Shipman et al., "A ferroelectric fast reactive tuner for superconducting cavities," *Proc. SRF2019*, Dresden, Germany, p. 781 (2019).
37. S. Cousineau, A. Rakhman, M. Kay, A. Aleksandrov, V. Danilov, T. Gorlov, Y. Liu, M. Plum, A. Shishlo, and D. Johnson, "First demonstration of laser-assisted charge exchange for microsecond duration H- beams." *Physical Review Letters* **118**, 078401 (2017).
38. E. Brunetti, W. Becker, H. C. Bryant, D A. Jaroszynski, and W. Chou, "Laser Stripping of Hydrogen Atoms by Direct Ionization", *New Journal of Physics* **17** 053008 (2015).